



Intratumoral and peritumoral radiomics based on dynamic contrast-enhanced MRI for preoperative prediction of intraductal component in invasive breast cancer

Hao Xu¹ · Jieke Liu¹ · Zhe Chen¹ · Chunhua Wang¹ · Yuanyuan Liu¹ · Min Wang¹ · Peng Zhou¹ · Hongbing Luo¹ · Jing Ren¹

Received: 19 August 2021 / Revised: 1 December 2021 / Accepted: 22 December 2021 / Published online: 25 January 2022

© The Author(s), under exclusive licence to European Society of Radiology 2022

Abstract

Objectives To develop and validate radiomic models for preoperative prediction of intraductal component in invasive breast cancer (IBC-IC) using the intratumoral and peritumoral features derived from dynamic contrast-enhanced MRI (DCE-MRI).

Methods The prediction models were developed in a primary cohort of 183 consecutive patients from September 2017 to December 2018, consisting of 45 IBC-IC and 138 invasive breast cancers (IBC). The validation cohort of 111 patients (27 IBC-IC and 84 IBC) from February 2019 to January 2020 was enrolled to test the prediction models. A total of 208 radiomic features were extracted from the intratumoral and peritumoral regions of MRI-visible tumors. Then the radiomic features were selected and combined with clinical characteristics to construct predicting models using the least absolute shrinkage and selection operator. The area under the curve (AUC) of receiver operating characteristic, sensitivity, and specificity were used to evaluate the performance of radiomic models.

Results Four radiomic models for prediction of IBC-IC were built including intratumoral radiomic signature, peritumoral radiomic signature, peritumoral radiomic nomogram, and combined intratumoral and peritumoral radiomic signature. The combined intratumoral and peritumoral radiomic signature had the optimal diagnostic performance, with the AUC, sensitivity, and specificity of 0.821 (0.758–0.874), 0.822 (0.680–0.920), and 0.739 (0.658–0.810) in the primary cohort and 0.815 (0.730–0.882), 0.778 (0.577–0.914), and 0.738 (0.631–0.828) in the validation cohort.

Conclusions The radiomic model based on the combined intratumoral and peritumoral features from DCE-MRI showed a good ability to preoperatively predict IBC-IC, which might facilitate the individualized surgical planning for patients with breast cancer before breast-conserving surgery.

Key Points

- Preoperative prediction of intraductal component in invasive breast cancer is crucial for breast-conserving surgery planning.
- Peritumoral radiomic features of invasive breast cancer contain useful information to predict intraductal components.
- Radiomics is a promising non-invasive method to facilitate individualized surgical planning for patients with breast cancer before breast-conserving surgery.

Keywords Breast neoplasms · Carcinoma, intraductal, noninfiltrating · Magnetic resonance imaging · Diagnostic imaging

Hao Xu and Jieke Liu contributed equally to this work.

✉ Hongbing Luo
rohbin@163.com

✉ Jing Ren
13880611648@163.com

¹ Department of Radiology, Sichuan Cancer Hospital & Institute, Sichuan Cancer Center, School of Medicine, University of Electronic Science and Technology of China, Chengdu, China

Abbreviations

ACR BI-RADS	American College of Radiology Breast Imaging Reporting and Data System
AUC	Area under the curve
BCS	Breast-conserving surgery
CI	Confidence interval
DCE-MRI	Dynamic contrast-enhanced MRI
DCIS	Ductal carcinoma in situ
ER	Estrogen receptor
ETL	Echo train length
FOV	Field of view

HER2	Human epidermal growth factor receptor 2
IBC	Invasive breast cancer
IBC-IC	Intraductal component in invasive breast cancer
IBSI	Image biomarker standardization initiative
ICC	Intraclass correlation coefficient
LASSO	Least absolute shrinkage and selection operator
NEX	Number of excitations
NME	Non-mass enhancement
ROC	Receiver operating characteristic
ROI	Region of interest
PR	Progesterone receptor
TA	Total acquisition time
TE	Echo time
TR	Repetition time
TRIPOD	Transparent reporting of a multivariable prediction model for individual prognosis or diagnosis statement

Introduction

Breast cancer is the most commonly diagnosed cancer among women [1, 2]. Breast-conserving surgery (BCS) followed by radiotherapy is now established as the “standard of care” for early-stage invasive breast cancer (IBC) [3, 4]. Emerging pieces of evidence suggest that positive surgical margins are correlated with the increased locoregional recurrence after BCS [5–7]. Therefore, the success of BCS relies on the clear surgical margins during initial tumor resection in a cosmetically acceptable manner [8].

The presence of an intraductal component (ductal carcinoma in situ, DCIS) in invasive breast cancer (IBC-IC) is a commonly mentioned risk factor that drives positive margin [9–11], re-operation rate [12, 13], and local-regional recurrence [7, 14] in BCS. Lack of imaging biomarkers for preoperatively identifying IBC-IC is the main cause for positive surgical margin and repetitive surgery [13]. MRI is an important imaging modality in locoregional management of breast cancer [15] and has been proven to be more sensitive and accurate than mammography and ultrasonography in detecting and depicting the extent of a given invasive cancer [16] and DCIS [17, 18]. Previous studies also indicated that preoperative MRI improved surgical planning and outcomes of patients with DCIS by depicting additional malignancy [18] and was associated with a lower risk of positive surgical margins in patients with IBC eligible for BCS [19].

Preoperative prediction of the presence of an intraductal component in a given tumor is crucial for surgical planning and outcome in breast cancer [20]. To date, some

researchers found that the MRI could improve the detection and depiction of the IBC-IC before surgery, compared with the other imaging modalities [21, 22]. Together with MRI-guided needle biopsy and MRI-guided surgery, MRI could contribute to improved surgical outcomes by reducing the positive margin during BCS [21]. However, evidence of the utility of radiomics based on dynamic contrast-enhanced MRI (DCE-MRI) to improve the preoperative prediction of IBC-IC, to our knowledge, is scarce. Radiomics refers to the science of converting medical images into high-throughput quantitative features, followed by subsequent data analysis and model building for clinical decision-making support [23]. MRI-based radiomics unravel an increasing number of mineable quantitative imaging biomarkers [24] and have been applied in breast cancer diagnosis [25, 26], molecular subtypes classification [27], therapeutic evaluation [28–30], early prognostic prediction [31–33], and recurrence risk prediction [34, 35], to stratify patients for precise and personalized care [36].

Therefore, we hypothesized that the intratumoral and peritumoral radiomic features derived from DCE-MRI might predict IBC-IC. The purpose of this retrospective study was to develop and validate radiomic models from two independent DCE-MRI protocols for preoperative prediction of IBC-IC.

Materials and methods

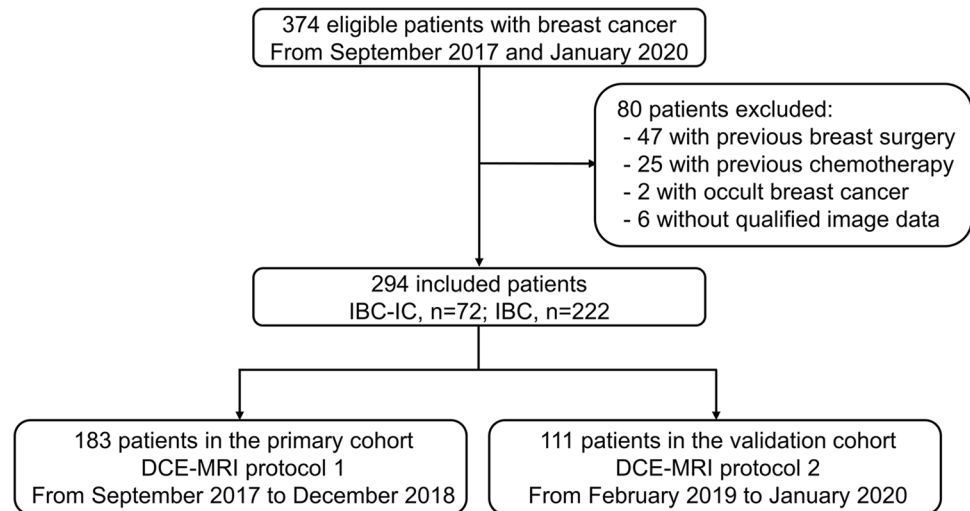
Patients

The retrospective analysis was approved by our institutional review board and the informed consent was waived. A total of 374 consecutive female patients between September 2017 and January 2020 were preliminarily enrolled in this study. The inclusion criteria were (1) patients with unilateral IBC confirmed by surgical pathology and (2) with DCE-MRI examination, which was the routine tool to aid breast surgeons for preoperative consulting and surgery planning in our institution. The exclusion criteria were (1) patients with previous breast surgery ($n = 47$), (2) with previous neoadjuvant or induction chemotherapy ($n = 25$), (3) with occult breast cancer ($n = 2$), and (4) without qualified image data ($n = 6$). Finally, a total of 294 patients were remained and divided into primary cohort (September 2017 to December 2018) and validation cohort (February 2019 to January 2020) according to two different MRI acquisition protocols (Fig. 1).

Histopathological analyses

Histopathology and immunohistochemistry data were directly obtained from the surgical pathology report. The

Fig. 1 Flowchart for patient recruitment in this study. *IBC-IC*, intraductal component in invasive breast cancer; *IBC*, invasive breast cancer; *DCE-MRI*, dynamic contrast-enhanced MRI



existence and status of the intraductal component were reviewed by two dedicated breast pathologists with 5 and 30 years of experience. All cases were thoroughly evaluated to identify the existence of the intraductal component from hematoxylin-eosin staining sections. Additional immunohistochemical staining (cytokeratin 5/6 and p63) was performed to differentiate intraductal components from invasive cancer. The status of the intraductal component including fraction and nuclear grade [37] was measured and documented as its ratio of the entire lesion (i.e., invasive plus intraductal part) [21]. In this study, IBC-IC was defined as the cases with DCIS component in or around invasive cancer (i.e., index cancer), while invasive cancer without DCIS component was defined as IBC. Estrogen receptor (ER) and progesterone receptor (PR) positivity was defined as the presence of 10% or more positively stained nuclei in 10 high-power fields. Human epidermal growth factor receptor 2 (HER2) expression was scored from 0 to 3: tumors with a score of 3 were classified as positive, tumors with a score of 0 or 1 were classified as negative, and tumors with scores of 2 were subjected to HER2 gene amplification by using chromogenic in situ hybridization to further confirm [31]. The threshold of high or low Ki-67 was defined as 14% [38].

MRI acquisition

All included patients underwent DCE-MRI on the 3.0 T scanner (Skyra, Siemens Healthcare) with a 16-channel breast coil. Gadodiamide (0.1 mmol/kg; Omniscan, GE Healthcare) was intravenously administered using a power injector (rate, 2.5 mL/s) before DCE-MRI. Then, a 20-mL saline flush was injected (rate, 2.5 mL/s). Two different ultrafast DCE-MRI protocols for radiomic model development and validation respectively were described as follows.

DCE-MRI protocol 1 The ultrafast DCE-MRI protocol for the primary cohort was performed between September 2017 and December 2018 which has been described in our previous studies [39, 40]. It included 26 consecutive phases using the commercially available CAIPIRINHA-Dixon-TWIST-VIBE sequence (Siemens Healthcare): repetition time (TR), 5.64 ms; echo time (TE), 2.46 ms; echo train length (ETL), 32; number of excitations (NEX), 1; field of view (FOV), 360 × 360 mm; slice thickness, 2.5 mm; no gap; matrix, 269 × 384; flip angle, 10°; acquisition type, 3D; temporal resolution, 12.0 s/phase; and total acquisition time (TA), 5 min 12 s. The images were reconstructed from the k-space using the inverse Fourier transform with interleaved stochastic trajectories method.

DCE-MRI protocol 2 The ultrafast DCE-MRI protocol for the validation cohort was performed between February 2019 and January 2020. It included 20 consecutive phases using the homemade sequence: TR, 5.06 ms; TE, 1.83 ms; ETL, 32; NEX, 1; FOV, 340 × 255 mm; slice thickness, 2.5 mm; no gap; matrix, 320 × 240; flip angle, 10°; acquisition type, 3D; temporal resolution, 16.6 s/phase; and TA, 5 min 33 s. The images were reconstructed from the k-space using the inverse Fourier transform with the linear filling method.

Image processing and segmentation

The 5th phase images of 26 dynamic phases in the primary cohort and the 4th phase images of 20 dynamic phases in the validation cohort were selected for processing and segmentation, which were equivalent to the first post-contrast images at the early arterial phase [41]. Then these images were preprocessed using the Artificial Intelligence Kit (A.K., version 3.2.0, GE Healthcare) software before segmentation. All images were firstly resampled to 1 × 1 × 1 mm³ isotropic voxels with a trilinear interpolation algorithm.

The position of the interpolation grid was aligned by the center and the dimensions of the interpolation grid were rounded to the nearest integer. Gaussian filter was used for anti-aliasing when down-sampling and the bias-field correction was also conducted. Then voxel intensity values were normalized with a z-score to eliminate the influence of the different ranges of gray values.

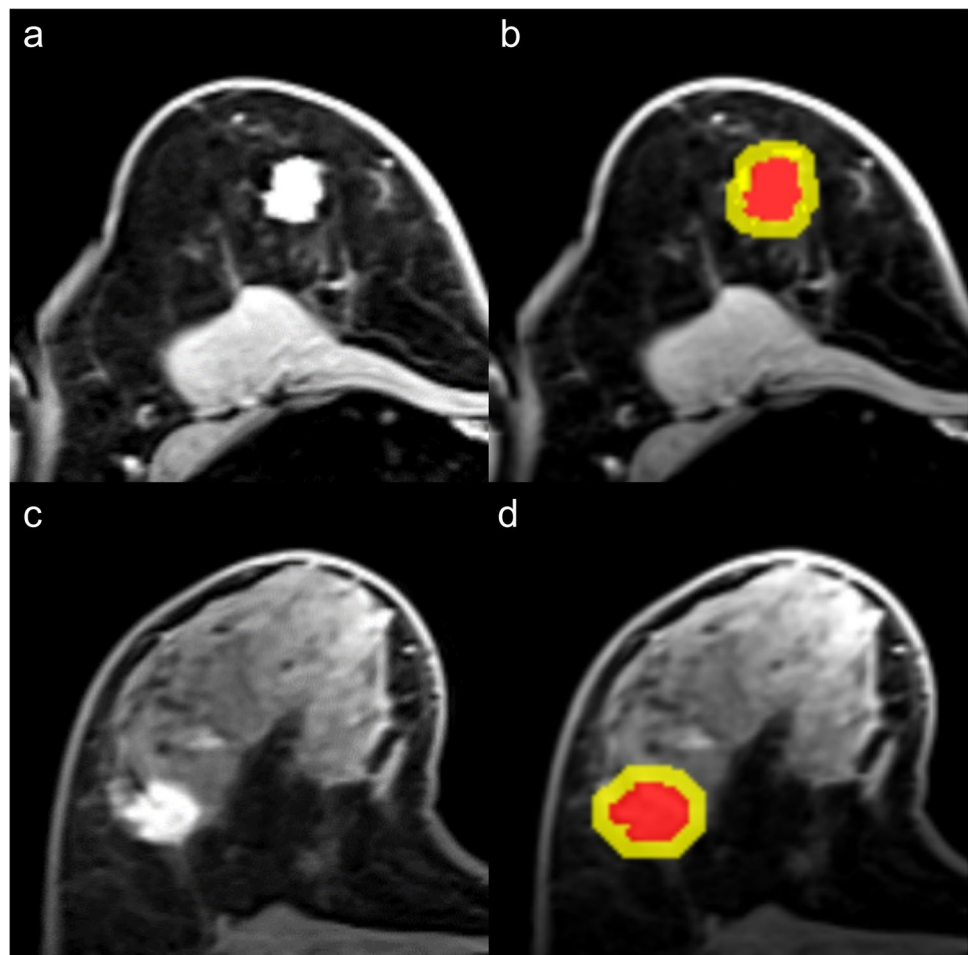
The region of interest (ROI) that covers the entire MRI-visible tumor (i.e., index tumor) was manually contoured slice by slice in axial plane using ITK-SNAP (version 3.8.0, <http://www.itksnap.org>). The largest tumor was selected as the index tumor when there were multiple lesions. The peritumoral regions were then obtained using the A.K. software by equidistant 3-dimensional dilation of the intratumoral regions with 4 mm [42–44]. The segmentations for all cases were performed by one radiologist with 5 years of experience in breast imaging. To assess inter-observer agreement, 30 randomly selected cases were segmented again by another radiologist with 15 years of experience in breast imaging. Both radiologists were blind to the clinical and histopathological data. The reliability was calculated using the intraclass correlation coefficient

(ICC). Features with ICCs greater than 0.75 indicated satisfactory reproducibility and were reserved for further analysis. The representative DCE-MRI images and the intratumoral and peritumoral ROIs are shown in Fig. 2.

Radiomic feature extraction

A total of 208 original features including shape, first order, and texture features were extracted from both the intratumoral and peritumoral ROIs (104 features for each) after image preprocessing and segmentation using an open-source Python package (PyRadiomics, version 3.0, <https://pyradiomics.readthedocs.io>) [45], which was basically compliant with the image biomarker standardization initiative (IBSI) standard [46]. A fixed bin number of 32 was used to discretize voxel intensity values before extracting texture features according to its good performance after z-score normalization in MRI [47]. Further details of radiomic features are provided in Supplementary Materials and Table S1-2.

Fig. 2 The representative dynamic contrast-enhanced MRI images and the intratumoral and peritumoral regions of interest. **a, b** A 63-year-old female with invasive breast cancer. **c, d** A 46-year-old female with intraductal component in invasive breast cancer



Radiomic feature selection and radiomic signature construction

Radiomic features were standardized using z-score normalization and then selected to build radiomic signatures based on intratumoral radiomic features, peritumoral radiomic features, and the combined intratumoral and peritumoral radiomic features respectively in the primary cohort. Then, a four-step feature selection methodology was performed. Firstly, the Mann-Whitney U test was conducted to select the features that were statistically different between patients with IBC-IC and IBC. The p value threshold for the remaining significant features was set at 0.05. Secondly, the Spearman correlation analysis was sequentially conducted to exclude redundant radiomic features. Highly correlated features (Spearman correlation coefficient > 0.9) were excluded. Thirdly, the least absolute shrinkage and selection operator (LASSO) method was used to select the most predictive features associated with IBC-IC in the primary cohort [48]. The radiomic signatures were calculated via a linear combination of the selected features and weighted by the respective coefficients. Spearman correlations were performed among the features in radiomic signatures to assess their multicollinearity. Feature selection and radiomic signature building were all performed using R software (version 4.0.0, <http://www.r-project.org>).

Model development and validation

Independent factors for differentiating IBC-IC from IBC among radiomic signatures and clinical variables were identified by inputting significant variables found in the primary cohort using univariate logistic regression analysis. Then a multivariable logistic regression analysis was applied to build a radiomic nomogram.

The discrimination performance of each model was assessed by the area under the curve (AUC) of receiver-operator characteristic (ROC) curve in both the primary and validation cohorts. The optimal threshold was determined by maximizing the Youden index. The sensitivity and specificity were also calculated. The binomial exact method was used to determine the confidence intervals (CIs) of the reported performance metrics. The Hosmer-Lemeshow (H-L) test was performed to assess the goodness-of-fit of predictive models. The calibration curve was also plotted and its corresponding calibration slope and calibration-in-the-large were measured [49].

MRI image analysis

All MRI images were retrospectively analyzed by two radiologists according to the American College of Radiology Breast Imaging Reporting and Data System (ACR

BI-RADS). Both radiologists were blinded to the pathological outcomes and assessed the following MRI morphologic features of each index tumor on the first post-contrast phase of DCE-MRI, including the lesion type (mass or non-mass enhancement, NME), lesion internal enhancement (homogeneous or heterogeneous), shape (oval/round or irregular), and margin (circumscribed or irregular/speculated) of masses. The disagreements between the two radiologists were resolved by consulting a third radiologist with 23 years of experience in breast imaging.

TRIPOD and statistical analysis

As a prediction model study for diagnostic purposes, this study followed the transparent reporting of a multivariable prediction model for individual prognosis or diagnosis (TRIPOD) statement [50].

Statistical analyses were performed using MedCalc (version 18.2.1, <https://www.medcalc.org>) and SPSS software (version 26.0, <https://www.ibm.com>). The independent sample t -test was used to compare the age between IBC-IC and IBC groups. The chi-square test or Fisher's exact test was conducted to analyze categorical variables including menopausal status, MRI morphologic features, and histopathological characteristics. The comparisons of AUCs between the predictive radiomic model with the highest AUC and the others were performed using the DeLong test in the primary and validation cohorts [51]. Further comparisons of sensitivity and specificity were performed using the McNemar test [52]. A two-tailed p value of <0.05 was considered statistically significant. The multiple comparisons were corrected using the Bonferroni method.

The association between IBC-IC and MRI morphologic features was further assessed using univariate logistic regression analysis. The prediction performance of the MRI morphologic features was assessed by the AUC of ROC curve and compared with that of the best radiomic model using the DeLong test [51].

Results

Demographic characteristics

A total of 294 patients including 72 (24.5%) IBC-IC patients and 222 (75.5%) IBC patients were recruited in this study. The MRI morphologic features and clinical and histopathological characteristics of patients in the primary and validation cohorts are summarized in Table 1. Significant differences were found in lesion type between the IBC-IC group and the IBC group in both primary and validation cohorts ($p < 0.001$ and $p = 0.009$). The IBC-IC patients were younger than IBC patients ($p = 0.012$) and

Table 1 MRI morphologic features and clinical and histopathological characteristics of patients in the primary and validation cohorts

Characteristics	Primary cohort (<i>n</i> = 183)			Validation cohort (<i>n</i> = 111)		
	IBC-IC (<i>n</i> = 45)	IBC (<i>n</i> = 138)	<i>p</i>	IBC-IC (<i>n</i> = 27)	IBC (<i>n</i> = 84)	<i>p</i>
Age (mean ± SD)	45.1 ± 8.1	49.4 ± 10.3	0.012	48.9 ± 8.8	51.1 ± 10.4	0.336
Menopausal status			0.223			0.792
Premenopausal	31 (68.9%)	81 (58.7%)		14 (51.9%)	46 (54.8%)	
Postmenopausal	14 (31.1%)	57 (41.3%)		13 (48.1%)	38 (45.2%)	
Lesion type			< 0.001			0.009
Mass	34 (75.6%)	132 (95.7%)		22 (81.5%)	82 (97.6%)	
Non-mass enhancement	11 (24.4%)	6 (4.3%)		5 (18.5%)	2 (2.4%)	
Lesion internal enhancement			0.270			0.568
Homogeneous	5 (11.1%)	25 (18.1%)		6 (22.2%)	14 (16.7%)	
Heterogeneous	40 (88.9%)	113 (81.9%)		21 (77.8%)	70 (83.3%)	
Mass shape*			0.737			0.999
Round or oval	2 (5.9%)	12 (9.1%)		3 (13.6%)	11 (13.4%)	
Irregular	32 (94.1%)	120 (90.9%)		19 (86.4%)	71 (86.6%)	
Mass margin*			0.013			0.820
Circumscribed	4 (11.8%)	44 (33.3%)		8 (36.4%)	32 (39.0%)	
Irregular or speculated	30 (88.2%)	88 (66.7%)		14 (63.6%)	50 (61.0%)	
Histological type			0.100			0.999
Invasive ductal carcinoma	45 (100.0%)	124 (89.9%)		27 (100.0%)	80 (95.2%)	
Invasive lobular carcinoma	0 (0.0%)	4 (2.9%)		0 (0.0%)	1 (1.2%)	
Others	0 (0.0%)	10 (7.2%)		0 (0.0%)	3 (3.6%)	
Molecular subtype			0.055			0.239
Luminal A	10 (22.2%)	24 (17.4%)		5 (18.5%)	12 (14.3%)	
Luminal B	21 (46.7%)	58 (42.0%)		15 (55.6%)	41 (48.8%)	
HER2 positive	10 (22.2%)	18 (13.0%)		6 (22.2%)	14 (16.7%)	
Triple negative	4 (8.9%)	38 (27.6%)		1 (3.7%)	17 (20.2%)	
ER			0.256			0.296
Positive	31 (68.9%)	82 (59.4%)		20 (74.1%)	53 (63.1%)	
Negative	14 (31.1%)	56 (40.6%)		7 (25.9%)	31 (36.9%)	
PR			0.270			0.116
Positive	29 (64.4%)	76 (55.1%)		20 (74.1%)	48 (57.1%)	
Negative	16 (35.6%)	62 (44.9%)		7 (25.9%)	36 (42.9%)	
HER2			0.044			0.726
Positive	20 (44.4%)	39 (28.3%)		9 (33.3%)	25 (29.8%)	
Negative	25 (55.6%)	99 (71.7%)		18 (66.7%)	59 (70.2%)	
Ki-67			0.326			0.418
Low	13 (28.9%)	30 (21.7%)		6 (22.2%)	13 (15.5%)	
High	32 (71.1%)	108 (78.3%)		21 (77.8%)	71 (84.5%)	

*Mass shape and margin were calculated with a denominator of 166 masses in the primary cohort and 104 in the validation cohort. Data are numbers of patients, with percentages in parentheses. *IBC-IC*, intraductal component in invasive breast cancer; *IBC*, invasive breast cancer; *SD*, standard deviation; *HER2*, human epidermal growth factor receptor 2; *ER*, estrogen receptor; *PR*, progesterone receptor

the proportion of irregular or speculated mass margin and HER2 positive in the IBC-IC group was higher than that in the IBC group ($p = 0.013$ and 0.044) in the primary cohort. But there were no significant differences in age, mass margin, and HER2 status in the validation cohort ($p = 0.336$, 0.820 , and 0.726). Additionally, there were no

significant differences in menopausal status, lesion internal enhancement, mass shape, histological type, molecular subtype, ER status, PR status, and Ki-67 between the IBC-IC and IBC groups in the primary and validation cohorts (all $p > 0.05$).

Radiomic feature selection and radiomic signature construction

Of the 208 extracted original radiomic features, 89 features from the intratumoral region and 55 features from the peritumoral region showed good inter-observer agreement (ICCs > 0.75). The process of radiomic features selection is presented in Supplementary Fig. S1-2. Finally, 4, 4, and 7 features were selected to construct intratumoral, peritumoral, and combined intratumoral and peritumoral radiomic signatures respectively. The mean and standard deviation of these features are provided in Supplementary Table S3 to conduct z-score normalization before calculation.

The calculation formula for intratumoral radiomic signature $\ln(P/1-P) = -1.357 - 0.0095 \times \text{shape_Flatness} - 0.8371 \times \text{shape_Sphericity} + 0.6066 \times \text{shape_SurfaceVolumeRatio} - 0.7562 \times \text{GLDM_LowGrayLevelEmphasis}$, where P is the probability of IBC-IC (cutoff > 0.1817).

The calculation formula for peritumoral radiomic signature $\ln(P/1-P) = -1.2048 - 0.4029 \times \text{shape_Flatness} + 0.2186 \times \text{firstorder_10Percentile} + 0.3995 \times \text{firstorder_RootMeanSquared} - 0.2168 \times \text{firstorder_TotalEnergy}$, where P is the probability of IBC-IC (cutoff > 0.2755).

The calculation formula for combined intratumoral and peritumoral radiomic signature $\ln(P/1-P) = -1.4034 - 0.9322 \times \text{intratumoral_shape_Sphericity} + 0.5822 \times \text{intratumoral_shape_SurfaceVolumeRatio} - 0.5794 \times \text{intratumoral_GLDM_LowGrayLevelEmphasis} + 0.2619 \times \text{peritumoral_firstorder_10Percentile} + 0.1189 \times \text{peritumoral_firstorder_Range} + 0.3665 \times \text{peritumoral_firstorder_RootMeanSquared} - 0.3933 \times \text{peritumoral_firstorder_TotalEnergy}$, where P is the probability of IBC-IC (cutoff > 0.2496).

The distributions of these radiomic signatures in the primary and validation cohorts are shown in Supplementary Fig. S3. The Spearman correlations among the features in these radiomic signatures are presented in Supplementary Table S4.

Model development and validation

Univariate logistic regression analysis found that IBC-IC was associated with age (OR = 0.954, $p = 0.013$). Further multivariate logistic regression analysis found that only age in the peritumoral dataset was associated with IBC-IC ($p = 0.041$) (Table 2). Therefore, the peritumoral radiomic nomogram was developed by integrating the peritumoral radiomic signature and age (Supplementary Fig. S4). The calculation formula for peritumoral radiomic nomogram is as follows: $\ln(P/1-P) = 2.0973 - 0.0410 \times \text{age} + 1.1666 \times \text{peritumoral radiomic signature}$, where P is the probability of IBC-IC (cutoff > 0.2374).

Finally, four radiomic models for prediction of IBC-IC were built including intratumoral radiomic signature, peritumoral radiomic signature, peritumoral radiomic nomogram, and combined intratumoral and peritumoral radiomic signature. The ROC curves of these radiomic models in the primary and validation cohorts are shown in Fig. 3. The AUC, sensitivity, and specificity of each radiomic model in the primary and validation cohorts are summarized in Table 3.

The calibration curves of intratumoral radiomic signature, peritumoral radiomic signature, peritumoral radiomic nomogram, and combined intratumoral and peritumoral radiomic signature showed good agreement between prediction and observation in both primary and validation cohorts (Supplementary Fig. S5), and the results of the Hosmer-Lemeshow test were insignificant

Table 2 Univariate and multivariate logistic regression analyses for predictive factors of IBC-IC in the primary cohort

Variables	Odds ratio	95% CI	<i>p</i>	
Univariate logistic analysis				
Age	0.954	0.920–0.990	0.013	
Intratumoral radiomic signature	3.201	1.989–5.152	< 0.001	
Peritumoral radiomic signature	3.410	1.846–6.298	< 0.001	
Combined intratumoral and peritumoral radiomic signature	3.493	2.220–5.496	< 0.001	
Multivariate logistic analysis				
Intratumoral radiomic nomogram	Age	0.968	0.930–1.008	0.119
	Radiomic signature	3.047	1.890–4.913	< 0.001
Peritumoral radiomic nomogram	Age	0.960	0.923–0.998	0.041
	Radiomic signature	3.211	1.730–5.961	< 0.001
Combined intratumoral and peritumoral radiomic nomogram	Age	0.970	0.929–1.013	0.168
	Radiomic signature	3.364	2.130–5.312	< 0.001

IBC-IC, intraductal component in invasive breast cancer; CI, confidence interval

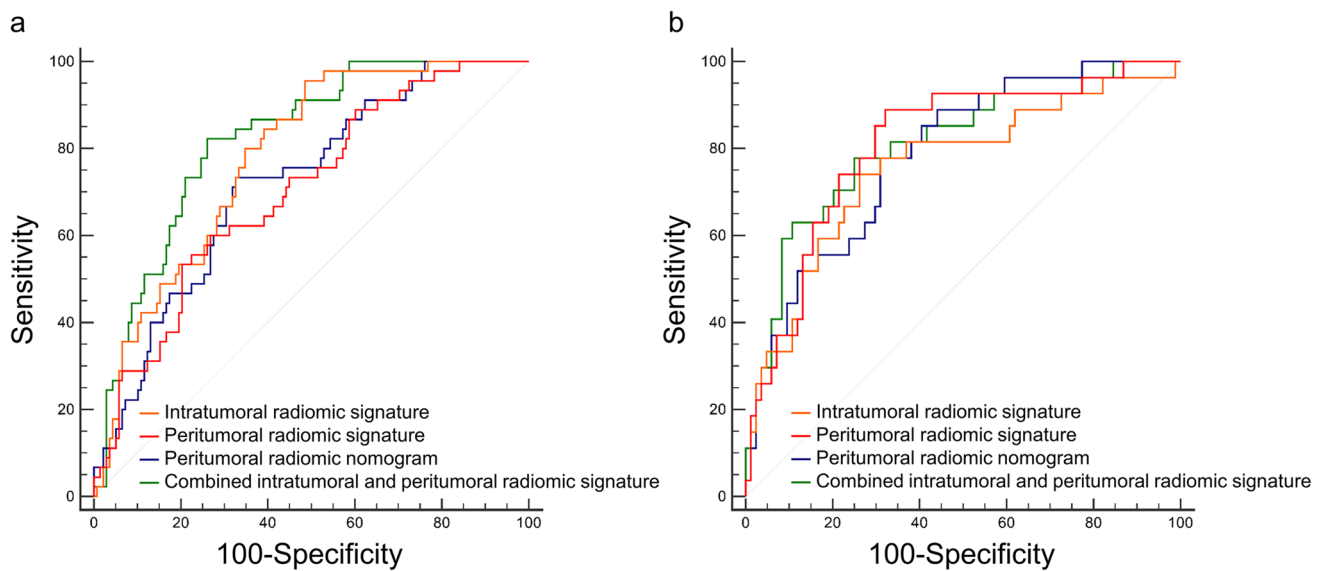


Fig. 3 Receiver operating characteristic curves of radiomic models for prediction of intraductal component in invasive breast cancer. **a** Primary cohort. **b** Validation cohort

Table 3 Diagnostic performance of radiomic models in the primary and validation cohorts

Models	Cohorts	AUC (95% CI)	Sensitivity	Specificity
Intratumoral radiomic signature	Primary	0.780 (0.712, 0.837)	0.956 (0.849, 0.995)	0.514 (0.428, 0.600)
	Validation	0.758 (0.667, 0.834)	0.815 (0.619, 0.937)	0.441 (0.332, 0.553)
Peritumoral radiomic signature	Primary	0.701 (0.629, 0.767)	0.600 (0.443, 0.743)	0.732 (0.650, 0.804)
	Validation	0.810 (0.725, 0.878)	0.852 (0.663, 0.958)	0.679 (0.568, 0.776)
Peritumoral radiomic nomogram	Primary	0.720 (0.649, 0.784)	0.733 (0.581, 0.854)	0.674 (0.589, 0.751)
	Validation	0.787 (0.700, 0.859)	0.815 (0.619, 0.937)	0.607 (0.495, 0.712)
Combined intratumoral and peritumoral radiomic signature	Primary	0.821 (0.758, 0.874)	0.822 (0.680, 0.920)	0.739 (0.658, 0.810)
	Validation	0.815 (0.730, 0.882)	0.778 (0.577, 0.914)	0.738 (0.631, 0.828)

AUC, the area under the curve; CI, confidence interval

($p = 0.324, 0.177, 0.219, 0.256$ in the primary cohort and $p = 0.873, 0.265, 0.800, 0.281$ in the validation cohort, respectively), which suggested no departure from a perfect fit.

Univariate logistic regression analysis revealed that lesion type was associated with IBC-IC (OR = 7.118, 95% CI = 2.457–20.622, $p < 0.001$). The lesion type yielded AUCs of 0.600 (0.526–0.672) in the primary cohort and 0.581 (0.483–0.674) in the validation cohort (Supplementary Fig. S6).

Comparison of models and TRIPOD

The combined intratumoral and peritumoral radiomic signature yielded the highest AUC among the radiomic models in both the primary and validation cohorts (AUC = 0.821, 95% CI = 0.758–0.874; AUC = 0.815, 95% CI = 0.730–0.882, respectively). According to the DeLong test, the AUC of the combined intratumoral and peritumoral radiomic signature was higher than that of the peritumoral radiomic signature and nomogram in the primary cohort ($p < 0.001$ and

$p = 0.006$), but not in the validation cohort ($p = 0.930$ and 0.626). There were no significant differences in the AUCs between the combined intratumoral and peritumoral radiomic signature and the intratumoral radiomic signature in the primary ($p = 0.080$) or validation cohort ($p = 0.056$) (Table 4). The McNemar test showed the specificities of the combined intratumoral and peritumoral radiomic signature in both the primary and validation cohorts were higher than those of the intratumoral radiomic signature (both $p < 0.001$). The sensitivity of the combined intratumoral and peritumoral radiomic signature was higher than that of the peritumoral radiomic signature in the primary cohort ($p = 0.006$), but not in the validation cohort ($p = 0.727$) (Table 4). The discriminating performances of the combined intratumoral and peritumoral radiomic signature in the primary and validation cohorts were superior to that of the lesion

type (0.821 vs. 0.600, $p < 0.001$; 0.815 vs. 0.581, $p < 0.001$, respectively). The representative images of the lesion type as mass and NME in IBC-IC and IBC groups are shown in Fig. 4.

We concluded the type of this study could be type 2b, and the TRIPOD checklist is presented in Supplementary Table S5.

Discussion

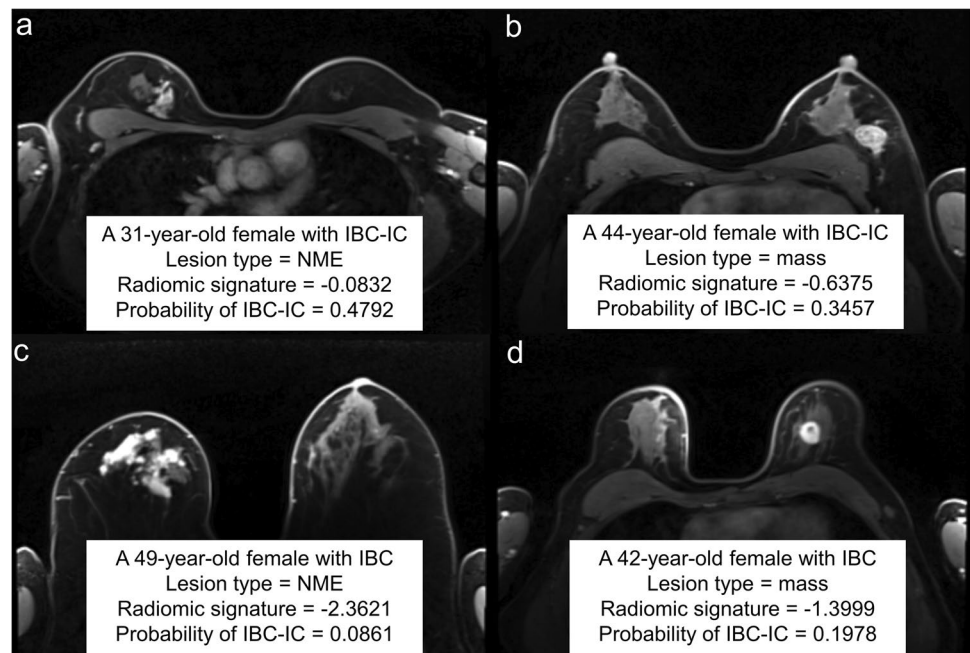
In this study, we developed and validated radiomic models incorporating intratumoral and peritumoral radiomic features for preoperative prediction of IBC-IC based on two different DCE-MRI protocols. The result showed the

Table 4 Comparisons of AUC, sensitivity, and specificity between the combined intratumoral and peritumoral radiomic signature and the other radiomic models in the primary and validation cohorts

Comparisons	AUC		Sensitivity		Specificity	
	Z	p	χ^2	p	χ^2	p
Primary cohort						
Intratumoral radiomic signature	1.750	0.080	3.125	0.070	29.032	< 0.001*
Peritumoral radiomic signature	3.371	< 0.001*	6.750	0.006*	0.000	0.999
Peritumoral radiomic nomogram	2.763	0.006*	1.125	0.289	0.164	0.163
Validation cohort						
Intratumoral radiomic signature	1.908	0.056	0.000	0.999	23.040	< 0.001*
Peritumoral radiomic signature	0.088	0.930	0.125	0.727	0.762	0.383
Peritumoral radiomic nomogram	0.488	0.626	0.000	0.999	3.704	0.052

*Differences were significant at $p < 0.05$ corrected with Bonferroni's method. AUC, the area under the curve

Fig. 4 a–d The representative images of the lesion type as mass and NME in IBC-IC and IBC groups. The radiomic signature was calculated from the combined intratumoral and peritumoral model and the cutoff probability for prediction of IBC-IC was 0.2496. NME, non-mass enhancement; IBC-IC, intraductal component in invasive breast cancer; IBC, invasive breast cancer



combined intratumoral and peritumoral radiomic signature had the optimal ability to preoperatively predict IBC-IC.

Preoperative prediction of IBC-IC based on DCE-MRI can help breast surgeons to optimize surgical planning before BCS. The incidence of IBC-IC is not rare in clinical practice. It was 24.5% (72/294) in our study, which was similar to previous literatures (20.6 to 52.6%) [21, 22, 53, 54]. IBC-IC is also a well-known risk factor that drives positive margin [9–11] and re-operation rate [13] in BCS. The published positive surgical margin rates in patients with IBC-IC ranged from 19.3 to 38.3% [55, 56] and the average re-operation rate was about 29.5% [13], which were both much higher than that in patients with pure IBC. Therefore, anticipating the IBC-IC before surgery can help surgeons appropriately define resection margins during BCS and reduce the rate of positive surgical margins [21] and incomplete resections [20]. Our results showed that the radiomic models based on DCE-MRI could non-invasively predict the presence of an intraductal component in patients with IBC before BCS, which might facilitate the personalized surgical planning for these patients. Together with MRI-guided needle biopsy and MRI-guided surgery, previous research demonstrated that the rate of positive surgical margins in IBC-IC patients could be reduced to 3.7% [21].

Traditional imaging researches found that the extensive IBC-IC often presented as ductal or linear enhancement, long spicules, a regional enhancing area, or nodules adjacent to a mass on MRI [22]. Compared the MRI findings with the histopathological examination, Van Goethem et al found that the peritumoral enhancement on MRI corresponded in 89.1% of cases with malignant extension by surgery pathology, and more than half of these correlated with DCIS [57]. Therefore, utilization of the peritumoral radiomic features may be helpful in the detection of IBC-IC. Previous studies showed that the early and overall peritumoral enhancement and amount of fibroglandular tissue around the MRI-visible tumor were associated with extensive IBC-IC, and the AUC of the prediction model based on these features was 0.79 [20]. These results are concordant with our results, suggesting that the peritumoral characteristics of breast tumors on MRI are of great help for the detection of IBC-IC. Recent studies have also demonstrated that the peritumoral radiomic features contained crucial information for breast cancer diagnosis [58], prognosis prediction [42, 44], and therapeutic evaluation [59]. As compared with the above studies, our study revealed that the combined intratumoral and peritumoral radiomic signature was the most optimal model among the radiomic models in predicting IBC-IC with the highest AUCs of 0.821 and 0.815 in both the primary and validation cohorts.

Our results also showed that the predictive performance of radiomic features was superior to the morphological features. Traditionally, morphological features of index tumor

on MRI are the only predictors for IBC-IC prediction, which are subject to visual interpretation. The traditional diagnostic mode is highly affected by the experience of radiologist. Thus, the performance for the prediction of IBC-IC based on morphological features ranged from 68 to 84.9% in previous literature [21, 22].

In the combined intratumoral and peritumoral radiomic signature, the intratumoral shape_Sphericity was negatively associated with IBC-IC and the intratumoral shape_SurfaceVolumeRatio was positively associated with IBC-IC, indicating that the masses of IBC-IC had less spherical and compact shape than that of IBC. The GLDM_LowGrayLevelEmphasis from the intratumoral region was negatively associated with IBC-IC, indicating that the masses of IBC-IC had less homogeneous textures with less concentration of low gray-level values. Besides, 4 first-order features from the peritumoral region including 10Percentile, Range, RootMeanSquared, and TotalEnergy were selected to construct the combined intratumoral and peritumoral radiomic signature. Our results suggested that the IBC-IC had a higher 10th percentile and range of gray level intensity, a higher square root of the mean of all the squared intensity values, and a lower sum of the squares of voxel values within the peritumoral region than IBC.

This study had several limitations. First, the retrospective design of this study had inherent selection bias. Second, the radiomic models in the study were developed and validated from two ultrafast DCE-MRI protocols using the same MRI scanner. Thus, the variance of radiomic features caused by different MRI scanners was not investigated. In addition, this was a single-center study. Hence, the radiomic models in this study need to be verified in a multicenter study with different imaging equipment in the future.

In conclusion, we developed and validated the radiomic model for preoperative prediction of IBC-IC based on the combined intratumoral and peritumoral features from DCE-MRI. This radiomic model provided the individualized probability of IBC-IC and might help to optimize surgical planning for patients with breast cancer before BCS.

Supplementary Information The online version contains supplementary material available at <https://doi.org/10.1007/s00330-022-08539-3>.

Acknowledgements The authors would like to thank Juan Ji (JJ) and Qiong Liao (QL) for the pathological work and consultation in the study.

Funding This study has received funding from Sichuan Science and Technology Program (grant numbers 2021YFG0125, 2021YFS0075, and 2021YFS0225).

Declarations

Guarantor The scientific guarantor of this publication is Hongbing Luo and Jing Ren.

Conflict of interest The authors of this manuscript declare no relationships with any companies whose products or services may be related to the subject matter of the article.

Statistics and biometry One of the authors has significant statistical expertise.

Informed consent The requirement for informed consent was waived and patient data are anonymized.

Ethical approval

Institutional Review Board approval was obtained.

Methodology

- Retrospective
- Diagnostic or prognostic study
- Performed at one institution

References

1. Siegel RL, Miller KD, Fuchs HE, Jemal A (2021) Cancer Statistics, 2021. *CA Cancer J Clin* 71:7–33
2. Sung H, Ferlay J, Siegel RL et al (2021) Global cancer statistics 2020: GLOBOCAN estimates of incidence and mortality worldwide for 36 cancers in 185 countries. *CA Cancer J Clin*. <https://doi.org/10.3322/caac.21660>
3. Sjöström M, Chang SL, Fishbane N et al (2019) Clinicogenomic radiotherapy classifier predicting the need for intensified locoregional treatment after breast-conserving surgery for early-stage breast cancer. *J Clin Oncol* 37:3340–3349
4. van Maaren MC, de Munck L, de Bock GH et al (2016) 10 year survival after breast-conserving surgery plus radiotherapy compared with mastectomy in early breast cancer in the Netherlands: a population-based study. *Lancet Oncol* 17:1158–1170
5. Marinovich ML, Azizi L, Macaskill P et al (2016) The association of surgical margins and local recurrence in women with ductal carcinoma in situ treated with breast-conserving therapy: a meta-analysis. *Ann Surg Oncol* 23:3811–3821
6. Houssami N, Macaskill P, Marinovich ML, Morrow M (2014) The association of surgical margins and local recurrence in women with early-stage invasive breast cancer treated with breast-conserving therapy: a meta-analysis. *Ann Surg Oncol* 21:717–730
7. Voogd AC, Nielsen M, Peterse JL et al (2001) Differences in risk factors for local and distant recurrence after breast-conserving therapy or mastectomy for stage I and II breast cancer: pooled results of two large European randomized trials. *J Clin Oncol* 19:1688–1697
8. Nayyar A, Gallagher KK, McGuire KP (2018) Definition and management of positive margins for invasive breast cancer. *Surg Clin North Am* 98:761–771
9. van Deurzen CH (2016) Predictors of surgical margin following breast-conserving surgery: a large population-based cohort study. *Ann Surg Oncol* 23:627–633
10. Bae MS, Bernard-Davila B, Sung JS, Morris EA (2019) Preoperative breast MRI features associated with positive or close margins in breast-conserving surgery. *Eur J Radiol* 117:171–177
11. Kang JH, Youk JH, Kim JA et al (2018) Identification of preoperative magnetic resonance imaging features associated with positive resection margins in breast cancer: a retrospective study. *Korean J Radiol* 19:897–904
12. Houvenaeghel G, Lambaudie E, Bannier M et al (2019) Positive or close margins: reoperation rate and second conservative resection or total mastectomy? *Cancer Manag Res* 11:2507–2516
13. Jeevan R, Cromwell DA, Trivella M et al (2012) Reoperation rates after breast conserving surgery for breast cancer among women in England: retrospective study of hospital episode statistics. *BMJ* 345:e4505
14. Schnitt SJ, Harris JR (2008) Evolution of breast-conserving therapy for localized breast cancer. *J Clin Oncol* 26:1395–1396
15. Kuhl CK, Lehman C, Bedrosian I (2020) Imaging in locoregional management of breast cancer. *J Clin Oncol* 38:2351–2361
16. Berg WA, Gutierrez L, Ness-Aiver MS et al (2004) Diagnostic accuracy of mammography, clinical examination, US, and MR imaging in preoperative assessment of breast cancer. *Radiology* 233:830–849
17. Kuhl CK, Schrading S, Bieling HB et al (2007) MRI for diagnosis of pure ductal carcinoma in situ: a prospective observational study. *Lancet* 370:485–492
18. Yoon GY, Choi WJ, Kim HH, Cha JH, Shin HJ, Chae EY (2020) Surgical outcomes for ductal carcinoma in situ: impact of preoperative MRI. *Radiology* 295:296–303
19. Gommers JJJ, Duijm LEM, Bult P et al (2021) The impact of preoperative breast MRI on surgical margin status in breast cancer patients recalled at biennial screening mammography: an observational cohort study. *Ann Surg Oncol*. <https://doi.org/10.1245/s10434-021-09868-1>
20. Knuttel FM, van der Velden BH, Loo CE et al (2016) Prediction model for extensive ductal carcinoma in situ around early-stage invasive breast cancer. *Invest Radiol* 51:462–468
21. Kuhl CK, Strobel K, Bieling H et al (2017) Impact of preoperative breast MR imaging and MR-guided surgery on diagnosis and surgical outcome of women with invasive breast cancer with and without DCIS component. *Radiology* 284:645–655
22. Van Goethem M, Schelfout K, Kersschot E et al (2007) MR mammography is useful in the preoperative locoregional staging of breast carcinomas with extensive intraductal component. *Eur J Radiol* 62:273–282
23. Gillies RJ, Kinahan PE, Hricak H (2016) Radiomics: images are more than pictures, they are data. *Radiology* 278:563–577
24. Bi WL, Hosny A, Schabath MB et al (2019) Artificial intelligence in cancer imaging: clinical challenges and applications. *CA Cancer J Clin* 5:21552
25. Li Z, Ai T, Hu Y et al (2018) Application of whole-lesion histogram analysis of pharmacokinetic parameters in dynamic contrast-enhanced MRI of breast lesions with the CAIPIRINHA-Dixon-TWIST-VIBE technique. *J Magn Reson Imaging* 47:91–96
26. Dijkstra H, Dorrius MD, Wielema M, Pijnappel RM, Oudkerk M, Sijens PE (2016) Quantitative DWI implemented after DCE-MRI yields increased specificity for BI-RADS 3 and 4 breast lesions. *J Magn Reson Imaging* 44:1642–1649
27. Xie T, Zhao Q, Fu C et al (2018) Differentiation of triple-negative breast cancer from other subtypes through whole-tumor histogram analysis on multiparametric MR imaging. *Eur Radiol* 6:018–5804
28. Drisis S, Metens T, Ignatiadis M, Stathopoulos K, Chao SL, Lemort M (2016) Quantitative DCE-MRI for prediction of pathological complete response following neoadjuvant treatment for locally advanced breast cancer: the impact of breast cancer subtypes on the diagnostic accuracy. *Eur Radiol* 26:1474–1484
29. Braman NM, Etesami M, Prasanna P et al (2017) Intratumoral and peritumoral radiomics for the pretreatment prediction of pathological complete response to neoadjuvant chemotherapy based on breast DCE-MRI. *Breast Cancer Res* 19:017–0846
30. Wu J, Gong G, Cui Y, Li R (2016) Intratumor partitioning and texture analysis of dynamic contrast-enhanced (DCE)-MRI identifies relevant tumor subregions to predict pathological response of breast cancer to neoadjuvant chemotherapy. *J Magn Reson Imaging* 44:1107–1115
31. Kim JY, Kim SH, Kim YJ et al (2015) Enhancement parameters on dynamic contrast enhanced breast MRI: do they correlate with

- prognostic factors and subtypes of breast cancers? *Magn Reson Imaging* 33:72–80
32. Pickles MD, Lowry M, Gibbs P (2016) Pretreatment prognostic value of dynamic contrast-enhanced magnetic resonance imaging vascular, texture, shape, and size parameters compared with traditional survival indicators obtained from locally advanced breast cancer patients. *Invest Radiol* 51:177–185
 33. Chang RF, Chen HH, Chang YC, Huang CS, Chen JH, Lo CM (2016) Quantification of breast tumor heterogeneity for ER status, HER2 status, and TN molecular subtype evaluation on DCE-MRI. *Magn Reson Imaging* 34:809–819
 34. Li H, Zhu Y, Burnside ES et al (2016) MR imaging radiomics signatures for predicting the risk of breast cancer recurrence as given by research versions of MammaPrint, Oncotype DX, and PAM50 gene assays. *Radiology* 281:382–391
 35. Park H, Lim Y, Ko ES et al (2018) Radiomics signature on magnetic resonance imaging: association with disease-free survival in patients with invasive breast cancer. *Clin Cancer Res* 24:4705–4714
 36. Pinker K, Chin J, Melsaether AN, Morris EA, Moy L (2018) Precision medicine and radiogenomics in breast cancer: new approaches toward diagnosis and treatment. *Radiology* 287:732–747
 37. Schuh F, Biazús JV, Resetskova E et al (2015) Histopathological grading of breast ductal carcinoma in situ: validation of a web-based survey through intra-observer reproducibility analysis. *Diagn Pathol* 10:93
 38. Goldhirsch A, Winer EP, Coates AS et al (2013) Personalizing the treatment of women with early breast cancer: highlights of the St Gallen International Expert Consensus on the Primary Therapy of Early Breast Cancer 2013. *Ann Oncol* 24:2206–2223
 39. Luo HB, Du MY, Liu YY et al (2020) Differentiation between luminal a and b molecular subtypes of breast cancer using pharmacokinetic quantitative parameters with histogram and texture features on preoperative dynamic contrast-enhanced magnetic resonance imaging. *Acad Radiol* 27:e35–e44
 40. Luo HB, Liu YY, Wang CH et al (2021) Radiomic features of axillary lymph nodes based on pharmacokinetic modeling DCE-MRI allow preoperative diagnosis of their metastatic status in breast cancer. *PLoS One* 16:e0247074
 41. Hao W, Zhao B, Wang G, Wang C, Liu H (2015) Influence of scan duration on the estimation of pharmacokinetic parameters for breast lesions: a study based on CAIPIRINHA-Dixon-TWIST-VIBE technique. *Eur Radiol* 25:1162–1171
 42. Liu C, Ding J, Spuhler K et al (2019) Preoperative prediction of sentinel lymph node metastasis in breast cancer by radiomic signatures from dynamic contrast-enhanced MRI. *J Magn Reson Imaging* 49:131–140
 43. Ding J, Chen S, Serrano Sosa M et al (2020) Optimizing the peritumoral region size in radiomics analysis for sentinel lymph node status prediction in breast cancer. *Acad Radiol*. <https://doi.org/10.1016/j.acra.2020.10.015>
 44. Li C, Song L, Yin J (2021) Intratumoral and peritumoral radiomics based on functional parametric maps from breast DCE-MRI for prediction of HER-2 and Ki-67 Status. *J Magn Reson Imaging*. <https://doi.org/10.1002/jmri.27651>
 45. van Griethuysen JJM, Fedorov A, Parmar C et al (2017) Computational radiomics system to decode the radiographic phenotype. *Cancer Res* 77:e104–e107
 46. Zwanenburg A, Vallieres M, Abdalah MA et al (2020) The image biomarker standardization initiative: standardized quantitative radiomics for high-throughput image-based phenotyping. *Radiology* 295:328–338
 47. Carré A, Klausner G, Edjlali M et al (2020) Standardization of brain MR images across machines and protocols: bridging the gap for MRI-based radiomics. *Sci Rep* 10:12340
 48. Sauerbrei W, Royston P, Binder H (2007) Selection of important variables and determination of functional form for continuous predictors in multivariable model building. *Stat Med* 26:5512–5528
 49. Steyerberg EW, Vickers AJ, Cook NR et al (2010) Assessing the performance of prediction models: a framework for traditional and novel measures. *Epidemiology* 21:128–138
 50. Moons KG, Altman DG, Reitsma JB et al (2015) Transparent reporting of a multivariable prediction model for individual prognosis or diagnosis (TRIPOD): explanation and elaboration. *Ann Intern Med* 162:W1–73
 51. DeLong ER, DeLong DM, Clarke-Pearson DL (1988) Comparing the areas under two or more correlated receiver operating characteristic curves: a nonparametric approach. *Biometrics* 44:837–845
 52. Hawass NE (1997) Comparing the sensitivities and specificities of two diagnostic procedures performed on the same group of patients. *Br J Radiol* 70:360–366
 53. Stomper PC, Connolly JL (1992) Mammographic features predicting an extensive intraductal component in early-stage infiltrating ductal carcinoma. *AJR Am J Roentgenol* 158:269–272
 54. Goh CW, Wu J, Ding S et al (2019) Invasive ductal carcinoma with coexisting ductal carcinoma in situ (IDC/DCIS) versus pure invasive ductal carcinoma (IDC): a comparison of clinicopathological characteristics, molecular subtypes, and clinical outcomes. *J Cancer Res Clin Oncol* 145:1877–1886
 55. Martin-Dunlap TM, Cyr AE, Al Mushawah F, Gao F, Margenthaler JA (2013) Does the volume of ductal carcinoma in situ impact the positive margin rate in patients undergoing breast conservation for invasive breast cancer? *J Surg Res* 184:228–233
 56. Chagpar AB, Killelea BK, Tsangaris TN et al (2015) A randomized, controlled trial of cavity shave margins in breast cancer. *N Engl J Med* 373:503–510
 57. Van Goethem M, Schelfout K, Kersschot E et al (2004) Enhancing area surrounding breast carcinoma on MR mammography: comparison with pathological examination. *Eur Radiol* 14:1363–1370
 58. Zhou J, Zhang Y, Chang KT et al (2020) Diagnosis of benign and malignant breast lesions on DCE-MRI by using radiomics and deep learning with consideration of peritumor tissue. *J Magn Reson Imaging* 51:798–809
 59. Braman NM, Etesami M, Prasanna P et al (2017) Intratumoral and peritumoral radiomics for the pretreatment prediction of pathological complete response to neoadjuvant chemotherapy based on breast DCE-MRI. *Breast Cancer Res* 19:57

Publisher's note Springer Nature remains neutral with regard to jurisdictional claims in published maps and institutional affiliations.